Accepted Manuscript

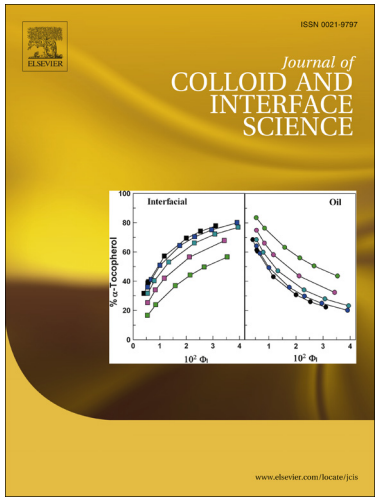

Regular article

Orientation of Charged Clay Nanotubes in Evaporating Droplet Meniscus

Yafei Zhao, Giuseppe Cavallaro, Yuri Lvov

PII: S0021-9797(14)00815-7
DOI: http://dx.doi.org/10.1016/j.jcis.2014.10.050
Reference: YJCIS 19944

To appear in: *Journal of Colloid and Interface Science*

Received Date: 19 September 2014
Accepted Date: 16 October 2014

Please cite this article as: Y. Zhao, G. Cavallaro, Y. Lvov, Orientation of Charged Clay Nanotubes in Evaporating Droplet Meniscus, *Journal of Colloid and Interface Science* (2014), doi: http://dx.doi.org/10.1016/j.jcis.2014.10.050

This is a PDF file of an unedited manuscript that has been accepted for publication. As a service to our customers we are providing this early version of the manuscript. The manuscript will undergo copyediting, typesetting, and review of the resulting proof before it is published in its final form. Please note that during the production process errors may be discovered which could affect the content, and all legal disclaimers that apply to the journal pertain.

ACCEPTED MANUSCRIPT

Orientation of Charged Clay Nanotubes in Evaporating Droplet Meniscus

Yafei Zhao[a], *Giuseppe Cavallaro*[b], *Yuri Lvov*[a, c, *1]
[a]Institute for Micromanufacturing, Louisiana Tech University, Ruston, USA
[b]Department of Physics and Chemistry, University of Palermo, Italy
[c]Kazan Federal University, Tatarstan, Russian Federation

Abstract
During drying, an aqueous suspension of strongly charged halloysite clay nanotubes concentrates at the edge of the droplet ("coffee-ring" effect) which provides alignment of the tubes along the liquid-substrate contact line. First, the surface charge of the nanotubes was enhanced by polyanion adsorption inside of the lumen to compensate for the internal positive charges. This increased the magnitude of the ξ-potential of the tubes from -36 to -81 mV and stabilized the colloids. Then, colloidal halloysite was dropped onto the substrate, dried at 65 °C and after a concentration of ~0.05 mg mL^{-1} was reached, the alignment of nanotubes occurred starting from the droplet edges. The process was described with Onsager's theory, in which longer nanorods, which have higher surface charge, give better ordering after a critical concentration is reached. This study indicates a new application of halloysite clay nanotubes in polymeric composites with anisotropic properties, microchannel orientation, and production of coatings with aligned nanotubes.

Keywords: halloysite nanotubes, alignment, droplet evaporation, coffee ring, liquid crystal

* Corresponding Author. Tel:1-318-257-5144. E-mail: ylvov@latech.edu

ACCEPTED MANUSCRIPT

1. Introduction

The self-assembly of nanoparticles is a perspective route to developing devices that exploit the properties of anisotropic materials properties, ranging from electronics to biomaterials. The controlled assembly of elongated particles such as carbon nanotubes, ZnO and DNA nanowires-allows for their preferential alignment along a spatial direction [1-4]. This process enhances the electrical, electrochemical, optical and electromechanical properties along the orientation line [2, 5-8]. Nano-fibers and tubes organize into ordered structures either through external stimuli or interparticle interactions; electrical, magnetic or mechanical forces, and liquid flow can induce the ordering [2, 5-6, 9-13]. Most of the methods based on external forces require specialized equipment and they are limited in their ability to fabricate uniformly aligned nanostructures over a large area. On the other hand, self-assembly can be achieved by specific interactions between the nano-objects as is used in spin coating, inject printing and drop casting [8-9, 14-18]. Recently, evaporation-induced self-assembly on solid surfaces has received attention due to the ease of fabricating highly organized structures [14-17]. Drying a droplet of nanoparticle dispersion drives the formation of ordered patterns on the substrate, which depends on the mode of solvent evaporation [17]. The pattern that is formed is often a ring-like deposit ("coffee ring") along the edge of the initial droplet. In absence of Marangoni flow and natural convection during evaporation, when the contact line of the drying droplet is pinned, there is an outward and radial hydrodynamic flow that prevents shrinkage of the droplet, which would replenish the liquid evaporating from the edge [17, 19]. This flow carries the suspended particles from the center to the droplet periphery, causing the formation of a dense ring-like deposition. When a critical colloid concentration is reached the anisotropic particles near the edge transition from the isotropic to the liquid crystal phase and align parallel to the edge, as was observed for carbon nanotubes [14, 20], gold [21] and iron oxide [22] nanoparticles. The explanation for this phenomenon is based on the classic Onsager's theory of high aspect ratio rigid rods forming orientation and position ordered liquid crystalline phases [1, 23]. A recent review [17] reported that the droplet-casting method was successfully used for the self-assembly of polymers, proteins, graphene and nanoparticles, such as carbon nanotubes and metal oxides. No results were yet reported for nanoclays, which are appealing natural materials for environmental friendly composites. Among the clays, halloysite is interesting for applications because of its large surface area, tunable surface chemistry and hollow tubular morphology [24-25].

Halloysite clay, which is rolled kaolinite sheets, has a tubular shape with different external and internal surface chemistry and high aspect ratio of about 10-30. The sizes of halloysite nanotubes (HNTs) are within 600-1500 nm in length, 10-20 nm in inner diameter, and 50-60 nm in outer diameter depending on the deposit and milling process. Halloysite has a positive alumina inner lumen and a negative silica outer surface allowing its selective functionalization [26-27] and the encapsulation of chemically and biologically active compounds [24-25, 28]. The toxicity of halloysite nanotubes was analyzed for human breast cells and human epithelial adenocarcinoma cells [29]. The viability of the halloysite-treated cells (up to 0.5 mg/mL) was preserved (up to 70% of viable cells), however, at higher concentrations of HNTs, cell death was induced. A low toxicity of chitosan-based scaffolds for tissue engineering was also demonstrated by monitoring the growth of fibroblasts on nanocomposites [30]. No significant effects of fibroblasts attachment and development on chitosan-doped scaffold were observed. Therefore, halloysite is considered as safe for very high concentration up 1 mg/mL of cell culture or tissue. These properties lead to halloysite application in functional polymeric composites with controlled release of anticorrosion, antimicrobial and flame-retardant agents and for wastewater treatment [24-25, 28, 31-36]. Halloysite can be dispersed in aqueous solutions by modifying the inner

ACCEPTED MANUSCRIPT

lumen with anionic–surfactants to greatly enhance the surface charge of the nanotubes [26-27]. Halloysite can form liquid crystalline phases when dispersed in aqueous solution [37].

Here we present a strategy to produce aligned halloysite structures by using evaporation-induced droplet-casting method. The nanotubes cavity was functionalized with poly(styrene sulfonate) to enhance its surface charge resulting in high colloidal stability which allows for the halloysite orientational self-assembly. The influence of the nanotubes length, charge and the concentration on orientation was analyzed. Onsager's theory and "coffee-ring" phenomenon were employed to explain the alignment self-assembly of halloysite nanotubes.

2. Experimental and Methods

2.1. Materials

Two types of halloysite nanotubes with different length were selected to observe the orientation phenomenon: halloysite with shorter length of ca 0.6 μm and length/diameter ratio of ca 15 which underwent to two-step milling was obtained from Applied Minerals Inc. (s-HNT), and none-milled pristine halloysite with full length of ca 1.5 μm and length/diameter ratio of ca 30 was purchased from China Henan Province (1-HNT). Polystyrene sulfonate sodium salt (PSS, MW 70,000) and sodium chloride (NaCl, 99.99%) were purchased from Sigma-Aldrich and were used without further treatments. Sodium hydroxide (NaOH, 1 M) and hydrochloric acid (HCl, 1M), prepared from analytical grade chemicals were purchased from Sigma-Aldrich and used for pH adjustments.

2.2. Preparation of PSS/HNTs hybrid for surface charge enhancing

2 g of PSS were dispersed in 100 mL of deionized water in a flask and stirred for 30 min to form a homogenous suspension. Then, s-HNTs or l-HNTs (2 g) were added gradually under continuous stirring in this solution, magnetically stirred for 48 h at room temperature and left standing for 1 h to precipitate aggregates. The individual HNTs were dispersed in the bulk, while the impurities and aggregations precipitated at the flask bottom. The supernatant dispersion was collected and then centrifuged at 5000 rpm for 10 min. The precipitated halloysite was washed 3-4 times with deionized water until it became neutral. Finally, the obtained solid was dried in a vacuum drier for 24 h and crushed into powder by mortar before use. The samples were denoted as PSS/s-HNTs and PSS/l-HNTs, respectively.

2.3. Droplet-casting method

Pristine HNTs and PSS-functionalized HNTs aqueous dispersions were prepared by adding HNTs, PSS/s-HNTs or PSS/l-HNTs into deionized water and ultrasonicated with power level of 70 watt per gallon for 5 min (the concentrations ranged from 0.01 to 100 mg mL^{-1}). These aqueous dispersions can be considered physically stable because the ξ-potential of both pristine and functionalized halloysite is above 30 mV (in absolute value). The "droplet-drying" process was carried out by dropping 20-100 μL of the dispersions onto a silicon wafer substrate and drying it at selected temperatures (25, 65, and 90 °C). Ionic force and pH of the dispersions were changed by adding NaCl, NaOH and HCl, respectively.

2.4. Instrumentation

2.4.1. Zeta-potential and dynamic light scattering

ξ-potential and dynamic light scattering (DLS) measurements were carried out by using

ACCEPTED MANUSCRIPT

microelectrophoretic ZetaPlus Potential Analyzer (Brookhaven Instruments) at 25.0 ± 0.1 °C. For this, diluted aqueous dispersions of pristine and functionalized halloysite (ca. 1 μg mL^{-1}) were transferred into the special cell and electric field was applied causing the movement of negatively charged nanotubes toward cathode. ξ-potential of the particles was determined by Smoluchowski formula. For all of the systems, the field-time autocorrelation functions were well described by a mono-exponential decay process, which provides the rate (Γ) correlated to the apparent diffusion coefficient $D_t = \Gamma/q^2$, where $q = 4\pi n\lambda^{-1}\sin(\theta/2)$ is the scattering vector, being n the water refractive index, θ the scattering angle (90°) and λ the wavelength (632.8 nm).

2.4.2. Thermogravimetry

Experiments were performed by using a TGA Q50 (TA Instruments) under nitrogen flow of 25 cm^3 min^{-1} for the sample and 10 cm^3 min^{-1} for the balance. The explored temperature interval ranged between 25 and 900 °C at a heating rate of 10 °C min^{-1}. The loading of the polymer in the PSS/HNTs hybrid was determined from the residual mass at 600 °C by taking into account the water content as reported in literature [26-27].

2.4.3. Contact angle

Contact angle experiments were performed by using an optical contact angle apparatus (OCA 20, Data Physics Instruments) equipped with a high-resolution CCD camera and a high-performance digitizing adapter. SCA 20 software (Data Physics Instruments) was used. For the study of the evaporation kinetics, a sessile droplet (volume was 10.0 ± 0.5 μL) of modified halloysite dispersion was deposited on the silicon wafer substrate. The concentration of the dispersion was 6 mg mL^{-1} and temperature 25.0 ± 0.1 °C both for the support and the injecting syringe. During the water evaporation, the evolution of the contact angle, contact radius and droplet volume were monitored. Images were collected 25 times per second up to 15 mins. The wettability of l-HNTs and PSS/l-HNTs solid pellets was also determined by measuring their initial contact angle with the sessile drop method.

2.4.4. Polarizing optical and scanning electron microscopies

The orientational processes were investigated using an Olympus BX-50 polarized light microscope under crossed polarizers during a 360° rotation of the sample. Images were captured with a microscope-mounted digital camera (Olympus C-4000 Zoom). After drying the droplet on silicon wafer, it was mounted on a specimen holder (stub) glued with carbon tap for scanning electron microscopy (SEM) observations in the secondary electron imaging mode by using HitachiS-4800 with an accelerating voltage of 3 kV. All the samples had been mildly annealed to reduce charging effects before being put into the SEM chamber. All SEM micrographs are related to the edge of the deposits.

3. Results and Discussion

3.1. Functionalization of halloysite

The colloidal stability of nanoparticles dispersion plays a crucial role on the efficiency of self-assembly by drop-casting [15]. We functionalized halloysite tube lumen with an anionic polymer, which is selectively adsorbed on the positive alumina surface of the nanotube innermost due to electrostatic interactions. Specifically, both long and short pristine halloysite nanotubes (1.5 μm l-HNTs and 0.5 μm s-HNTs) were modified with poly (styrene sulfonate) (PSS). The polymer loading was 5.1 ± 0.5 wt. %, which indicates that the nanotubes are almost fully filled with PSS considering that the halloysite lumen is ca. 10 % of the tube hole. The addition of PSS does not change the surface wettability of the clay (Table 1) and pristine and inner-functionalized clay nanotubes possess similar hydrophilicity. This finding proves the selective modification of the halloysite inner surface (the

ACCEPTED MANUSCRIPT

presence of PSS on the outer surface would determine an increase of the nanoparticles' hydrophobicity because of the polymer chains). Moreover, table 1 shows that the diffusion coefficient $\boldsymbol{D_t}$ of both short and long nanotubes is not influenced by the PSS functionalization indicating that the hybrids do not aggregate in agreement with the absence of hydrophobic attractive interactions generated by the chains of PSS. This makes the modified halloysite suitable for self-assembly by drop-casting. ξ-potential data revealed that charge of clay nanotubes is not influenced by their length, while the modification with PSS determined an increase of the net negative charge. This result agrees with the entrapment of the anionic polymer into the halloysite lumen and neutralization of its inner positive charges. Similar findings were observed for anionic surfactants/HNTs hybrids [26-27]. Based on the Derjaguin and Landau, Verwey and Overbeek (DLVO) theory [38], the increase of halloysite ξ-potential after the modification improves the colloidal stability of the nanorods because of the enhancement of the repulsive interactions. Both long and short pristine halloysite nanotubes (l-HNTs and s-HNTs) aqueous dispersions of 10 mg mL^{-1} started to precipitate after 1 hour, and almost all tubes sediment after 12 hrs, *e.g.* the original halloysite clay nanotube colloids were unstable (Fig. 1a). However, after modification with PSS, no halloysite precipitation or aggregation occurred during the first hours and only tiny sediment appeared after 24 hrs allowing for stable colloidal dispersion for more than four weeks. SEM analysis of PSS/l-HNTs droplet on silicon wafer after complete drying showed the high quality of the alignment at the droplet edge (Fig. 1b). This indicated on the sufficient dispersion stability of PSS/HNTs for self-assembly.

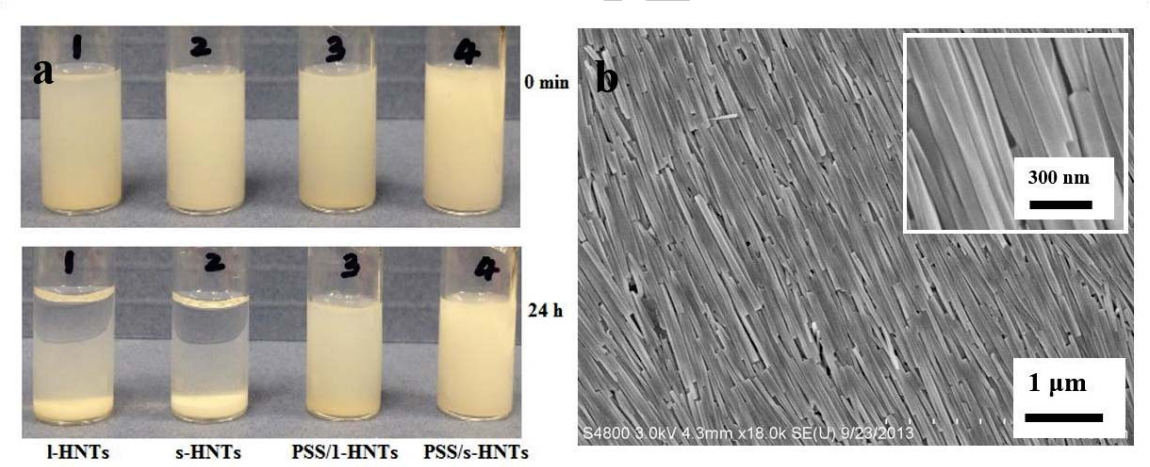

Figure 1. (a) Images of pristine and modified halloysite dispersion after 0 and 24 hrs, (b) SEM images of PSS/l-HNTs film after water evaporation in the edge of the droplet on silicon substrate.

Table 1. Physico-chemical properties of pristine and PPS modified halloysite (s-short and l-long), data error 5 %

Materials	$D_t \times 10^{12}$ / m^2 s^{-1}	ξ-potential / mV	Initial water contact angle / °
s-HNTs	1.1	-38	20
PSS/s-HNTs	1.1	-81	20
l-HNTs	1.2	-36	21
PSS/l-HNTs	1.1	-64	21

ACCEPTED MANUSCRIPT

3.2. Evaporation of halloysite droplet on substrate

Drops of isotropic phase of pristine and PSS-modified halloysite were placed onto silicon substrate to study self-organized structures of the nanotubes. Optical micrographs of dried droplets (Fig. 2a) indicate the formation of a "coffee-ring" deposit in the periphery due to the outward capillary flow that occurs during the water evaporation. Typically, the film thickness for dried droplets at the coffee ring edge was 3.5 ± 0.5 μm, in the center 1.0 ± 0.2 μm and droplet diameter was 2.5 ± 0.5 mm.

This phenomenon is ascribable to the pinning of the contact line between the droplet and the substrate which agrees well with the evaporation kinetics. The contact angle and the volume decrease linearly over time, while the droplet contact radius was constant (Fig. 2b-c). These trends indicate that the three-phase contact line is steadily pinned to the solid substrate as the drop evaporates. The hydrodynamic flow into the droplet drives the dispersed nanotubes to the edge concentrating suspension around the rim. Namely, if the droplet consists of a dilute suspension of pristine or functionalized HNTs, many of the nanotubes will be shuttled toward the droplet edge, increasing the local concentration there.

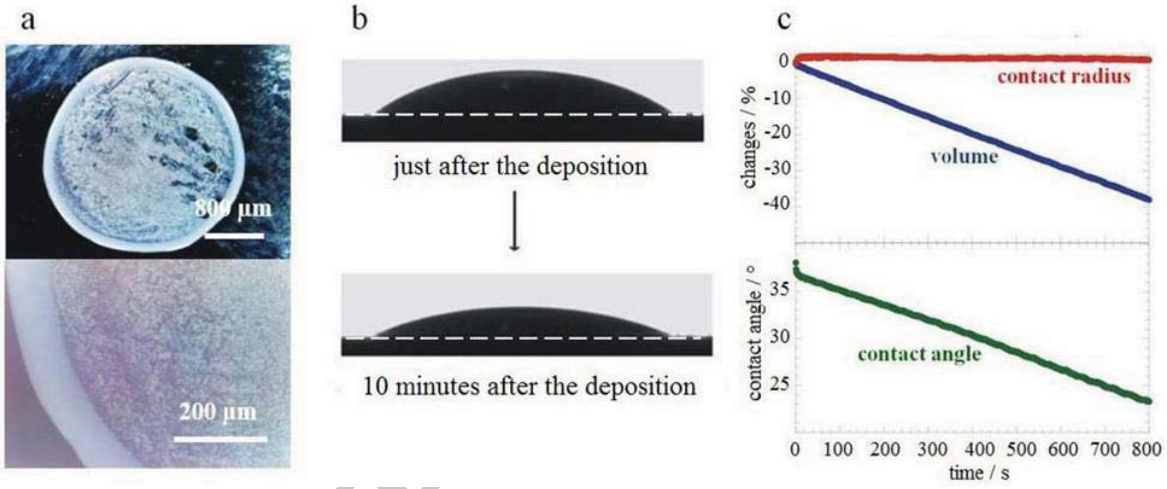

Figure 2. Droplet evaporation of 10 μL droplets for 6 mg mL^{-1} PSS/l-HNTs dispersions on a silicon wafer. (a) Optical micrographs of droplet after complete evaporation (b) Images of droplets for PSS/l-HNTs dispersion during the evaporation. (c) Dependence of volume, contact radius and contact angle of the droplet on time. These data were collected until the proper interpolation of the droplet contact line was clearly carried out.

When the local concentration at the droplet periphery increases up to a critical value the nanotubes may transition to a liquid crystalline phase and will also align parallel to the edge [20]. The parallel orientation is mostly due to the development of a flow-induced torque on the nanotubes as one of their ends becomes pinned by the contact line and, therefore, their axial flow directions change to parallel to the edge because of the geometrical constraints (Fig. 3). This is due to the frictional force between the substrate and the tubes in suspension coupled with accelerated evaporation at the contact line. The alignment of the first nanotubes that reach the edge is due to their induced torque rotation [20, 41]. Once this happens, other nanotubes from the suspension can accumulate onto the halloysite already located on the triple line upon evaporation of the liquid [41]. The ordering from the periphery to the inner region can be obtained by increasing the nanotubes' concentration beyond the critical value, as expressed by the Onsager theory.

ACCEPTED MANUSCRIPT

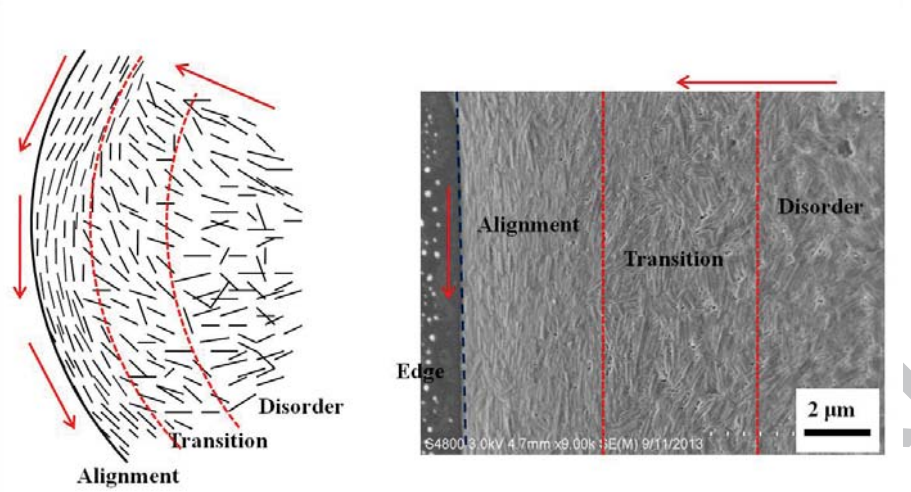

Figure 3. Sketch of the flow for halloysite nanotubes and correspondent SEM images of the sections of the dried dispersion droplet.

3.3. Liquid crystalline phase

Fig. 4 shows the formation of a ring-like liquid crystalline deposit along the perimeter of the droplet. The birefringence observed over the ring area indicates the presence of a nematic liquid crystalline phase with aligned nanotubes. The dark region in the center shows the isotropic phase (disordered). The different degree of ordering moves from the center to the edge. Fig. 4b highlights the transient isotropic/nematic region toward the edge of the dried droplet.

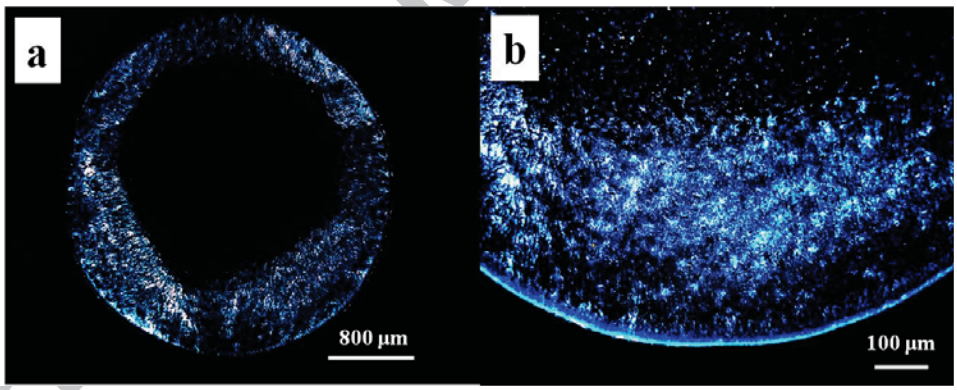

Figure 4. Polarized optical images of PSS/l-HNTs at 6 mg mL^{-1} after the droplet 65° C drying (a-whole view and b-edge section).

The topological defects in the orientation, referred as disclinations, have been identified as common and distinctive characteristics in liquid crystal. The disclination pattern further indicates the transition from isotropic to liquid crystal phase during evaporation. Namely, the nanotubes are aligned to form the director pattern around the disclination core (Fig. 5). On the basis of Frank elastic continuum theory [39], the disclinations represent arrangements of minimum energy and they are distinguished by their strength (***m***), which corresponds to the number of rotations (in multiples of 2π) over a path encircling the disclination, and a valve of constant parameter (***p***), which relates the axial position in the plane around the disclination core (polar angle ***θ***) and the director orientation angle ***φ***: the equation $\varphi(\theta) = m\theta + p$ is appropriate for the simplest case and it is generally used for the characterization of the disclinations in liquid crystal films [40]. According to this equation, for a two-dimensional ordered

ACCEPTED MANUSCRIPT

liquid crystal there are two types of disclinations with half integer strength (***m*** = ± 1/2): one positive (the parabolic disclination) and one negative (the hyperbolic disclination). On the other hand, for ***m*** = ± 1 one negative pattern (hyperbolic with 4-fold symmetry) and three positive patterns (radial, circular and spiral can be expected. The energy related to the disclinations depends on m^2. Therefore, the half-integer strength disclinations are topologically more stable than the integer defects [12, 22]. Fig. 5 reports the types of disclinations observed for dried deposits of PSS/l-HNTs. The most of disclinations possess **m** = ±1/2 in agreement with their higher stability (Fig. 5a-c). The presence of few disclinations with **m** = +1 (Fig. 4d-f**)** could be due to the impurities or short broken tubes in the center of the core that stabilize the defects against the energetically favored dissociation **m**(+1) → **m**(+1/2) + **m**(+1/2) [15]. The latter can be attributed to high polydispersion of halloysite.

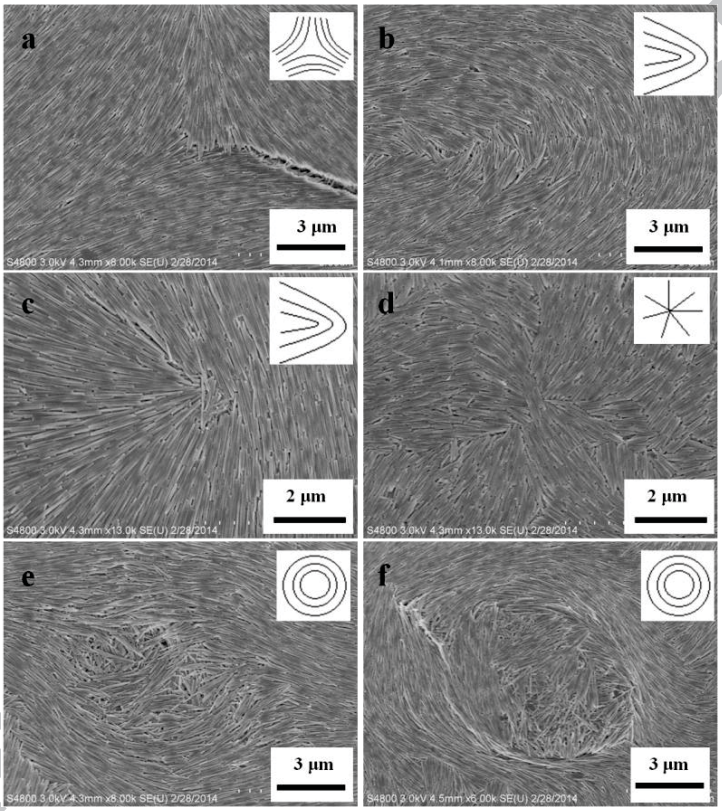

Figure 5. SEM images of axial disclinations in dried droplet of PSS/l-HNTs, concentration 20 mg mL^{-1}, drying at 65 ºC; (a) the hyperbolic disclination, *m* = -1/2, (b-c) the parabolic disclination, *m* = +1/2, (d- f) the circular and the spiral disclinations *m* = +1.

3.4. Clay nanotubes self-assembly by drop-castings

In order to understand the mechanism controlling the self-assembly of the clay nanotubes during the droplet evaporation, we investigated the effects of the halloysite concentration, length, surface charge, pH and salt addition, and temperature.

3.4.1. Effect of particles' concentration

The degree of alignment was highly dependent on the initial concentration of the nanotube dispersions. At very low concentration of 0.01 mg mL^{-1}, PSS/l-HNTs did not assemble into ordered phases (Fig. 6a). Rods/tubes dispersion must reach a critical concentration for transition from isotropic to nematic phase and be self-assembled at the three-phase contact line (interface between vapor, substrate and solution) as the solvent evaporated [23, 42]. Considering that the majority of nanotubes in dispersion

ACCEPTED MANUSCRIPT

condensed in the "coffee-ring", the critical concentration should be the minimum amount which ensures an effective assembly in the edge region. We found that to obtain a complete alignment, the initial concentration must be above *ca.* 0.05 mg mL^{-1}. Interestingly, the ordering is favored at higher concentration (Fig. 6b-d). This is in contrary to the ordering results for carbon nanotubes and may be attributed to the rigidness and straightness of halloysite nanotubes [20]. A higher concentration increases the number of nanotubes at the contact line, thus amplifying the frictional force between the solution and the substrate. The larger frictional force requires a larger capillary force in the contact line, resulting in wider ring and better alignment from edge to center of the droplet [16].

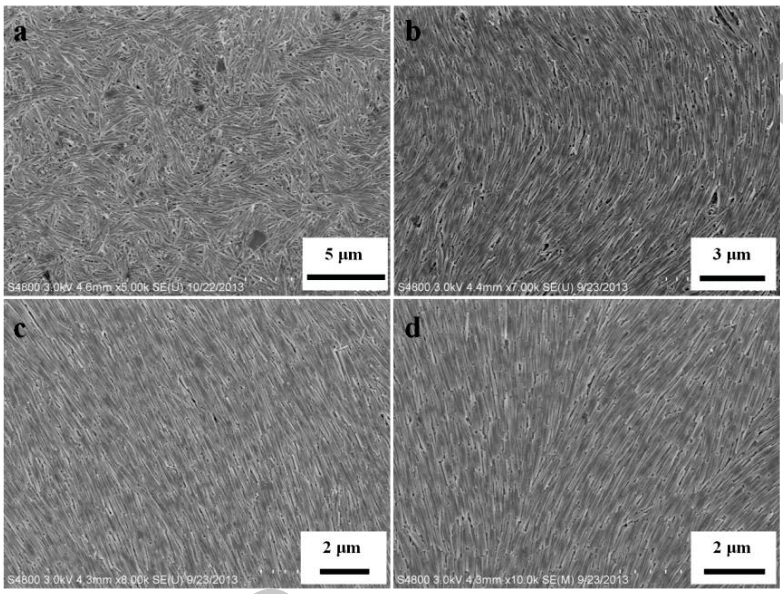

Figure 6. SEM images of the dried droplet edge of PSS/ l-HNTs at different concentrations: (a) 0.01, (b) 0.1, (c) 10, and (d) 100 mg mL^{-1} (drying temperature 65 ºC).

3.4.2. Effect of the tubes' length and charge

Fig. 7 shows typical SEM micrographs for the distribution and alignments of pristine and PSS-modified (strongly charged) halloysite after droplet drying. Both short and long pristine halloysite nanotubes (lower charged with ξ-potential of -36 mV) were randomly distributed after the water evaporation (Fig. 7a-b). On the other hand, PSS-modified halloysite nanotubes with ξ = -81 mV have showed higher ordering degree. PSS/s-HNTs organized into short range ordered alignment, while a better organization was found for longer PSS-l/HNTs (Fig. 7 c-d). Similar results were observed in suspensions of shorter and longer carbon nanotubes [20, 43]. These observations are in agreement with the Onsager's theory [42] by considering that the excluded volume interactions between the tubes in a given volume are dependent on their length. Namely, the critical concentration for the isotropic/nematic transition decreases with the length of the nanotubes. The entropy of the nematic phase is maximized with the long-range orientation of the nanotubes.

For better understanding, we determined the orientational order parameter $\boldsymbol{S}$ for PSS-modified halloysite from high magnification SEM images. Considering a two dimensional (2D) system, $\boldsymbol{S} = \mathbf{2\cos^2\varphi - 1}$, where $\boldsymbol{\varphi}$ is the average angle between the optimal aligned direction and the main tube axis. The orientational order parameter $\boldsymbol{S}$ ranges between -1 and 1 with large absolute values representing higher order. The sign of $\boldsymbol{S}$ is positive if the nanotubes tend to align parallel to the average orientation and negative if they tend to orient perpendicular to it. We calculated $\boldsymbol{S}$ = 0.56 and $\boldsymbol{S}$ = 0.90 for short and long PSS modified halloysite. Given that for monodisperse uncharged and rigid rods the Onsager

ACCEPTED MANUSCRIPT

theory predicts $S \approx 0.7$ at the isotropic/nematic transition [42], we concluded that long nanotubes functionalized with PSS show a very high degree of ordering (nematic phase) in a large scale range. This result can be attributed to the enhancement of the halloysite surface charge that affect the excluded volume interactions between the nanotubes and, consequently, the orientational ordering.

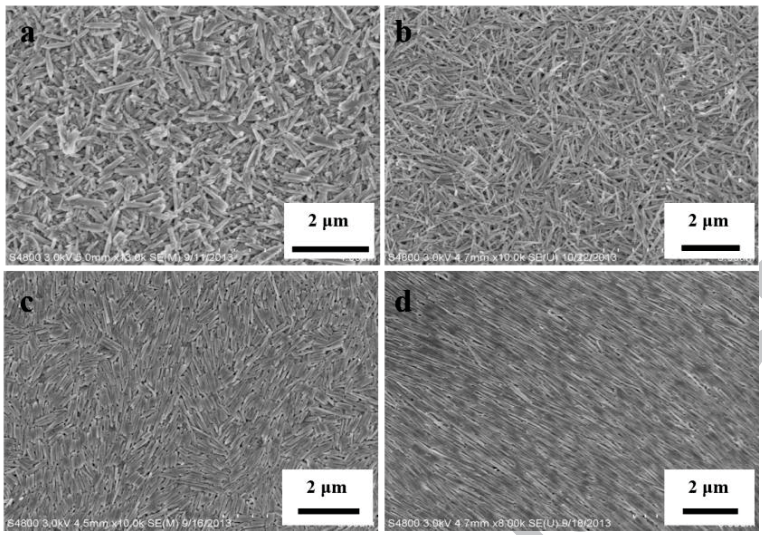

Figure 7. SEM images of the dried droplet edge, concentration 6 mg mL^{-1}, drying temperature 65 ºC: pristine low charge (a) s-HNTs, and (b) l-HNTs; enhanced charge tubes (c) PSS/s-HNTs, (d) PSS/l-HNTs;

3.4.3. Effect of pH and ionic strength

pH of halloysite aqueous dispersions is a crucial factor for the nanotubes alignment. Long l-HNTs display a disordered pattern at pH = 3 - 4 because the SiO_2 surface of halloysite is discharged (halloysite isoelectric point is 3.5). The tube ξ-potential is ±15 mV at pH 3-4, which is much lower than the colloidal stability of ±30 mV. However, when pH is above 5, the tube ξ-potential reached minus 70-80 mV and highly ordered structures were formed. These results suggest that the halloysite self-alignment highly depends on its charge and colloidal stability. This is attributed to columbic repulsion between negatively charged tubes, preventing random agglomeration and allowing for space and time for tubes' alignment. Nanotube aggregation at low pH can be reversed by tuning the solution pH back up to 5-6 with diluted NaOH and mild sonication. No difference in the halloysite dispersions was identified when the pH was raised to 5 and up to pH 9 which is in agreement with constant ξ-potential of -80 mV in this region (Fig. 8).

ACCEPTED MANUSCRIPT

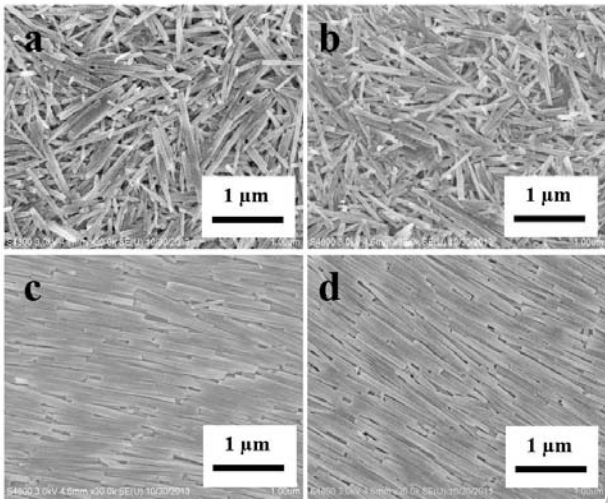

Figure 8. SEM images of the dried droplet of 6 mg mL^{-1}; PSS/l-HNTs dried at 65 ºC, at variable pH: (a) 3, (b) 4, (c) 5, (d) 9.

Increasing of ionic strength plays a similar role for nanotubes alignment diminishing columbic repulsion. This also determined a reduction of PSS/l-HNTs ordering (Fig. 9) due to the screening effect of the salt on the nanotubes. An addition into the halloysite dispersion of 0.1 M NaCl destroyed an orientation of the nanotubes in agreement with decline of the ξ-potential from -81 mV to -25 mV. The colloids were destabilized and tubes randomly aggregated in a few minutes after addition of NaCl.

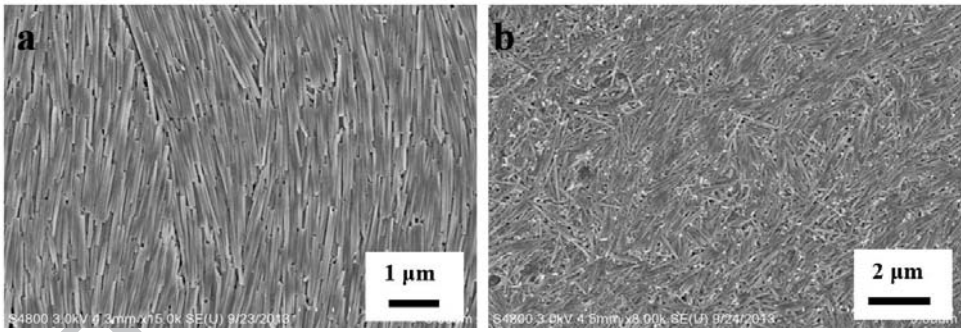

Figure 9. SEM images of the dried droplet edge of PSS/l-HNT tubes (a) without NaCl and (b) with 0.1 M of NaCl (concentration 6 mg mL^{-1}, drying temperature 65 ºC).

3.4.4. Effect of temperature

The evaporation temperature has a profound effect on the formation of the nematic phase of the tubes. Slow evaporation rate at low temperature (25 ºC) leads to random aggregation in the internal region outside of the "coffee-ring" area. In contrast, the faster evaporation at temperature of 60-90 ºC leads to good tube alignment in the whole droplet area (Fig. 10). This may be related with kinetic effect and competition between entropic and energetic driving forces. The rotational and translational diffusion constants **(D_i)** for rod-shaped particles in dispersion rely on temperature as $D_i \propto T/\eta_s$, where η_s is the shear viscosity. Since η_s decreases with increase in temperature, self-assembly becomes faster, effectively giving the system more time to lower its free energy. So, the improvement in alignment with elevating temperature indicates that the parallel aligned tubes are thermodynamically stable. It is well-known that hard rod-shaped particles in the droplet spontaneously undergo a transition to orientational ordering when the solvent volume shrinks due to evaporation, because the gain in

ACCEPTED MANUSCRIPT

positional entropy (associated with reducing the total excluded volume) is more than the loss in rotational entropy.

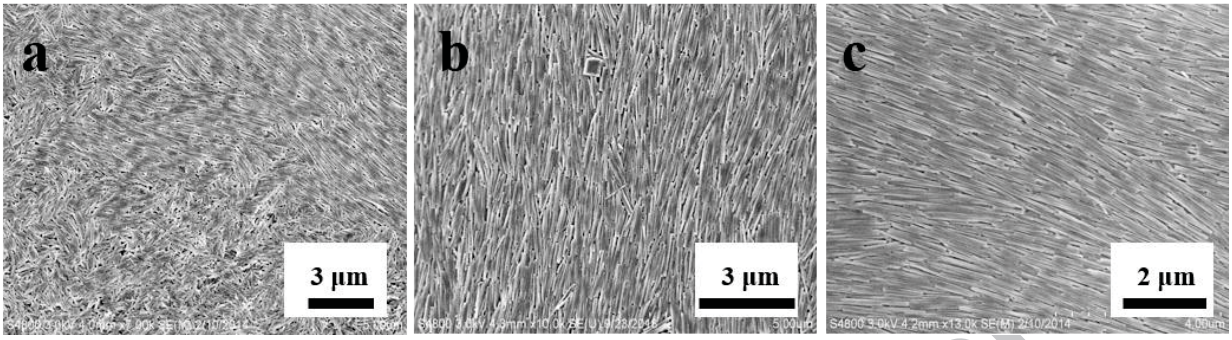

Figure 10. SEM images of the dried droplet of 6 mg mL^{-1} PSS/l-HNTs dried at variable temperature: (a) 25 ºC, (b) 65 ºC, (c) 90 ºC.

3.4.5. Applications for capillary orientation

To demonstrate the utility of the technique to control the clay nanotube orientation we fabricated continuous aligned layers using evaporation technique with capillary and shear forces. First, microchannels with 10 µm depth and 100 µm width were fabricated onto silicon wafers substrate by Reactive Ion Etching (RIE) method in clean room. A large droplet of the nanotubes dispersion on the top of 100-µm microchannel pattern resulted in aligned nanotubes along the periodic microchannels after evaporation. Second, a microfluidic device was created by pressing 5-µm channel silicon wafer into PDMS plate then covered by glass slide. Droplets of halloysite dispersion was injected into the PDMS microchannels resulting in high degree of alignment of the nanotubes in the direction along the channels after drying (Fig. 11). During drying, all nanotubes contained in the droplet deposit on the substrate and are assembled on the PDMS stripes generating multilayered superstructures of densely packed nanoclays. This process is due to the fact that most of the particles are transported to the edge of the droplet and, therefore, the nanotubes come into contact with each other under the influence of capillary forces. Moreover, the entropic interactions should be considered to explain the alignment along the stripes [42]. For higher particles' density, the nanotubes assemble side by side in order to minimize the excluded volume reducing the orientation entropy [42]. The scale range of the orientational ordering depends on the concentration of the aqueous suspension. Fig 11b shows the formation of multilayers of aligned nanotubes moving from the PDMS stripe-substrate interface to the center of the PDMS channel. Similar multilayers structures were reported for spherical [44] and tubular [45] gold particles.

ACCEPTED MANUSCRIPT

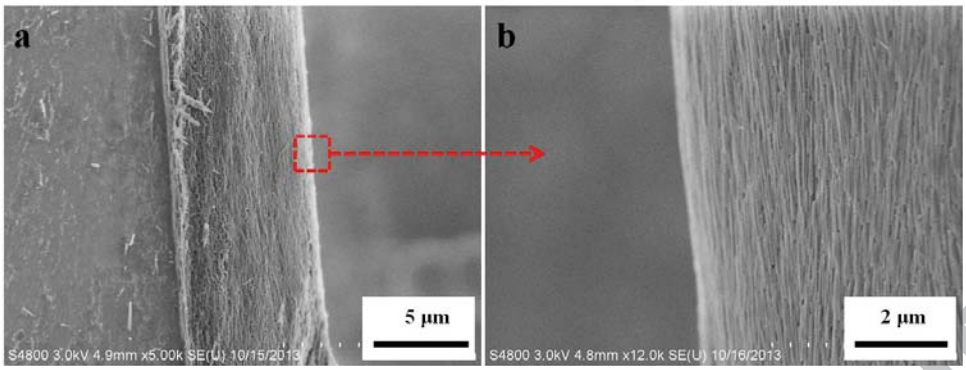

Figure 11. SEM images of PSS/l-HNTs films oriented in 5-μm channel, concentration 100 mg mL^{-1}.

PDMS mold technique allowed to design different micropatterns for studying alignment of the nanotubes. A thin PDMS film with round shape cut off was bonded onto the silicon substrate, followed by dropping of nanotube dispersions and drying. When the PDMS mold was removed, well-ordered arrays of nanotubes were observed on the silicon wafer within the designed spots. It would be very interesting to get the nanotube alignment by pen writing with halloysite ink because the nanotubes have tendency to align along mechanical shear force direction. This approach may be a simple method for printing of aligned nanostructures. All the above techniques have to be accomplished with controlled evaporation process.

3.5. Thermodynamic of the halloysite nanotubes orientational phenomena

The halloysite clay nanotube alignment can be explained by the Onsager theory [1, 23, 42]. It states that the isotropic to nematic phase transition stems from the competition of rotational and translational entropy. In the diluted suspension, each nanotube can move freely without restricting by neighboring tubes, resulting in random orientation and maximum rotational and translational entropy. With the increase of the concentration, the randomly oriented nanotubes crowd together limiting their translational freedom. The total entropy is maximized by aligning the nanotubes when critical concentration is reached, increasing the translational entropy by sacrificing the orientational one. The critical concentration ($c_{i\text{-}n}$) required for the isotropic-nematic transition is expressed by the following equation [42]

$$c_{i\text{-}n} = 16/(\pi L^2 D_{\text{eff}}) \quad (1)$$

where $c_{i\text{-}n}$ is the critical concentration expressed as number density, L is the length and D_{eff} is the effective electrostatic diameter, which takes into account the nanorods charge. Given that the isotropic-nematic transition is a dynamic process, the ordering of halloysite is favored for longer nanotubes. D_{eff} of charged rods is larger than that of uncharged rods by an amount proportional to Debye screening length. Consequently, the enhancement of the halloysite surface charge determines an increase of D_{eff} shifting to longer range the average distance between the nanotubes. Accordingly, the modification of halloysite cavity with PSS, which causes a large increase of halloysite ξ-potential, leads to ordering because of the very strong repulsive interactions between the nanotubes. Within this, the influence of pH and ionic strength on the nanotubes alignment is crucial: for pH ≥ 5, D_{eff} is larger favoring the tubes ordering. An increase of the ionic strength determines a decrease of D_{eff} (because of the screening effect), and the nanotubes alignment is disadvantageous.

ACCEPTED MANUSCRIPT

4. Conclusions

With droplet-casting method, we obtained highly ordered patterns of halloysite nanotubes. An evaporation of a droplet of halloysite isotropic dispersion on wettable substrate determines the formation of a "coffee-ring" deposit due to the pinning of the contact line, and halloysite nanotubes are aligned along the edge. The presence of disclinations on the deposited pattern confirms the transition from isotropic to liquid crystal phase during solvent evaporation. The concentration of the nanotube aqueous dispersion is crucial to determine the ordering on the rim. The degree of alignment may be controlled by changing the length and the charge of the nanotubes as well as by the ionic strength and pH of the solvent. We demonstrated that the modification of the halloysite inner cavity with anionic poly(styrene sulfonate) leads to better ordering because of an enhancement of net negative charge of the nanotubes. Accordingly, the self-assembly of the clay nanotubes is favored at basic pH, while the increase of the ionic strength causes opposite effects by screening the tube's surface charge. The mechanism controlling the halloysite nanotube ordering is explained with Onsager's theory as well. The evaporation induced clay nanotubes orientation in microchannels was also demonstrated. Although our approach has some limitations, it was the first time to obtain orientation halloysite nanotubes film and it would give a meaningful guide for explanation and application of aligned halloysite nanotubes.

Acknowledgments

We are thankful to Dr. G. Lazzara (Palermo University, Italy) and Dr. W. Wei (LaTech) for help in the experimental work and results discussion. The authors acknowledge support by NSF-1029147, NSF EPS-1003897 and FIRB 2012 (prot. RBFR12ETL5) grants. Any opinions, findings, and conclusions or recommendations expressed in this report are those of authors and do not necessarily reflect the view of National Science Foundation. This work was partially funded by the Russian Government Program of Competitive Growth of Kazan Federal University among World's Leading Academic Centers.

References

[1] Li, Y. G.; Wu, Y. Y. Coassembly of Graphene Oxide and Nanowires for Large-Area Nanowire Alignment. *J. Am. Chem. Soc.* **2009**, *131*, 5851–5857.

[2] Sun, B. Q.; Sirringhaus, H. Surface Tension and Fluid Flow Driven Self-Assembly of Ordered ZnO Nanorod Films for High-Performance Field Effect Transistors. *J. Am. Chem. Soc.* **2006**, *128*, 16231-16237.

[3] Byrne, N.; Menzies, D.; Goujon N.; Forsyth, M. Inducing Alignment of Cyclic Peptide Nanotubes Through the Use of Structured Ionic Liquids. *Chem. Commun.* **2013**, *49*, 7729-7731.

[4] Tian, Z. R.; Voigt, J. A.; Liu, J.; Mckenzie, B.; Xu, H. F. Large Oriented Arrays and Continuous Films of TiO_2-Based Nanotubes. *J. Am. Chem. Soc.* **2003**, *125*, 12384-12385.

[5] Lee, S. H.; Lee, H. J.; Ino, K.; Shiku, H.; Yao, T.; Matsue, T. Microfluid-Assisted Dielectrophoretic Alignment and Device Characterization of Single ZnO Wires. *J. Phys. Chem. C* **2009**, *113*, 19376-19381.

[6] Li, X. L.; Zhang, L.; Wang, X. R.; Shimoyama, I.; Sun, X. M.; Seo, W. S.; Dai, H. J. Langmuir-Blodgett Assembly of Densely Aligned Single-Walled Carbon Nanotubes from Bulk Materials. *J. Am. Chem. Soc.* **2007**, *129*, 4890-4891.

ACCEPTED MANUSCRIPT

[7] Mclean, R. S.; Huang, X. Y.; Khripin, C.; Jagota, A.; Zheng, M. Controlled Two-Dimensional Pattern of Spontaneously Aligned Carbon Nanotubes. *Nano Lett.* **2006**, *6*, 55-60.

[8] Li, B.; Han, W.; Byun, M.; Zhu, L.; Zou, Q. Z.; Lin, Z. Q. Macroscopic Highly Aligned DNA Nanowires Created by Controlled Evaporative Self-Assembly. *ACS Nano* **2013**, *7*, 4326–4333.

[9] Grzelczak, M.; Vermant, J.; Furst, E. M.; Liz-Marzán, L. M. Directed Self-Assembly of Nanoparticles. *ACS Nano* **2010**, *4*, 3591–3605.

[10] Shaver, J.; Parra-Vasquez, A. N. G.; Hansel, S.; Portugall, O.; Mielke, C. H.; Ortenberg, M. V.; Hauge, R. H.; Pasquali, M.; Kono, J. Alignment Dynamics of Single-Walled Carbon Nanotubes in Pulsed Ultrahigh Magnetic Fields. *ACS Nano* **2009**, *3*, 131–138.

[11] Klinov, D.; Atlasov, K.; Kotlyar, A.; Dwir, B.; Kapon, E. DNA Nanopositioning and Alignment by Electron-Beam-Induced Surface Chemical Patterning. *Nano Lett.* **2007**, *7*, 3583–3587.

[12] Zhou, H.; Heyer, P.; Kim, H. J.; Song, J. H.; Piao, L. H.; Kim, S. H. Reversible Macroscopic Alignment of Ag Nanowires. *Chem. Mater.* **2011**, *23*, 3622–3627.

[13] Olszowka, V.; Hund, M.; Kuntermann, V.; Scherdel, S.; Tsarkova L.; Böker, A. Electric Field Alignment of a Block Copolymer Nanopattern: Direct Observation of the Microscopic Mechanism. *ACS Nano* **2009**, *3*, 1091–1096.

[14] Beyer S. T.; Walus, K. Controlled Orientation and Alignment in Films of Single-Walled Carbon Nanotubes Using Inkjet Printing. *Langmuir* **2012**, *28*, 8753−8759.

[15] Zhang, S. J.; Li, Q. W.; Kinloch I. A.; Windle, A. H. Ordering in a Droplet of an Aqueous Suspension of Single-Wall Carbon Nanotubes on a Solid Substrate. *Langmuir* **2010**, *26*, 2107–2112.

[16] Shastry, T. A.; Seo, J. W. T.; Lopez, J. J.; Arnold, H. N.; Kelter, J. Z.; Sangwan, W. K.; Lauhon, L. J.; Marks, T. J.; Hersam, M. C. Large-Area, Electronically Monodisperse, Aligned Single-Walled Carbon Nanotube Thin Films Fabricated by Evaporation-Driven Self-Assembly. *Small* **2013**, *9*, 45–51.

[17] Han, W.; Lin, Z. Learning from "Coffee Rings": Ordered Structures Enabled by Controlled Evaporative Self-Assembly. *Angew Chem Int Ed Engl.* **2012**, *51*, 1534-1546.

[18] Liu, Y.; Zhao, X. L.; Cai, B.; Pei, T. F.; Tong, Y. H.; Tang, Q. X.; Liu, Y. C. Controllable Fabrication of Oriented Micro/Nanowire Arrays of Dibenzo-Tetrathiafulvalene by a Multiple Drop-casting Method. *Nanoscale* **2014**, *6*, 1323-1328.

[19] R. D. Deegan, O. Bakajin, T. F. Dupont, G. Huber, S. R. Nagel, T. A. Witten, Capillary Flow as the Cause of Ring Stains from Dried Liquid Drops. *Nature*, **1997**, *389*, 827–829.

[20] Li Q. W.; Zhu, Y. T. Self-Organization of Carbon Nanotubes in Evaporating Droplets. *J. Phys. Chem. B* **2006**, *110*, 13926-13930.

[21] Ma, H. M.; Dong, R. H.; Horn, J. D. V.; Hao, J. C. Spontaneous Formation of Radially Aligned Microchannels. *Chem. Commun.* **2011**, *47*, 2047–2049.

[22] Byun, M.; Wang, J.; Lin, Z. Q. Massively Ordered Microstructures Composed of Magnetic Nanoparticles. *J. Phys.: Condens. Matter*. **2009**, *21*, 264014.

[23] De Gennes, P. G. The Physics of Liquid Crystals, Oxford University Press, London, 1974, pp. 6-374.

[24] Lvov, Y. M.; Shchukin, D. G.; Möhwald H.; Price, R. R. Halloysite Clay Nanotubes for Controlled Release of Protective Agents. *ACS Nano* **2008**, *2*, 814–820.

[25] Lvov, Y. M.; Abdullayev, E. Functional Polymer-Clay Nanotube Composites with Sustain Release of Chemical Agents. *Prog. Polym. Sci.* **2013**, *38*, 1690-1719.

[26] Cavallaro, G.; Lazzara, G.; Milioto, S. Exploiting the Colloidal Stability and Solubilization Ability of Clay Nanotubes/Ionic Surfactant Hybrid Nanomaterials. *J. Phys. Chem. C* **2012**, *116*,

ACCEPTED MANUSCRIPT

21932–21938.

[27] Cavallaro, G.; Lazzara, G.; Milioto, S.; Parisi, F.; Sanzillo. V. Modified Halloysite Nanotubes: Nanoarchitectures for Enhancing the Capture of Oils from Vapor and Liquid Phases. *ACS Appl. Mater. Interfaces* **2014**, *6*, 606-612.

[28] Abdullayev, E.; Sakakibara, K.; Okamoto, K.; Wei, W. B.; Ariga, K.; Lvov, Y. M. Natural Tubule Clay Template Synthesis of Silver Nanorods for Antibacterial Composite Coating. *ACS Appl. Mater. Interfaces* **2011**, *3*, 4040–4046.

[29] Vergaro, V.; Abdullayev, E.; Lvov, Y. M.; Zeitoun, A.; Cingolani, R.; Rinaldi, R.; Leporatti, S. Cytocompatibility and Uptake of Halloysite Clay Nanotubes. *Biomacromolecules* 2010, *11*, 820-826.

[30] Liu, M. X.; Wu, C. C.; Jiao, Y. P.; Xiong S.; Zhou, C. R. Chitosan–Halloysite Nanotubes Nanocomposite Scaffolds for Tissue Engineering. *J. Mater. Chem. B*, **2013**, *1*, 2078-2089.

[31] Abdullayev, E.; Joshi, A.; Wei, W. B.; Zhao, Y. F.; Lvov, Y. M. Enlargement of Clay Nanotube Lumen by Selective Etching of Aluminum Oxide. *ACS Nano* **2012**, *6*, 7216-7226.

[32] Yah, W. O.; Takahara, A.; Lvov, Y. M. Selective Modification of Halloysite Lumen with Octadecyl Phosphonic Acid: New Inorganic Tubular Micelle. *J. Am. Chem. Soc.* **2012**, *134*, 1853-1859.

[33] Du, M.; Guo, B.; Jia D. Newly Emerging Applications of Halloysite Nanotubes. *Polymer Intern.* **2010**, *59*, 574-95.

[34] Zhao, Y. F.; Abdullayev, E.; Vasiliev, A.; Lvov, Y. M. Halloysite Nanotubule Clay for Efficient Water Purification. *J. Colloid Interface Sci.* **2013**, *406*, 121–129.

[35] Zhai, R.; Zhang, B.; Wan, Y. Z.; Li, C. C.; Wang, J. T.; Liu, J. D. Chitosan-Halloysite Hybrid-Nanotubes: Horseradish Peroxidase Immobilization and Applications in Phenol Removal. *Chem. Engineer. J.* **2013**, *214*, 304-309.

[36] Liu, L.; Wan, Y. Z.; Xie, Y. D.; Zhai, R.; Zhang, B.; Liu, J. D. The Removal of Dye from Aqueous Solution using Alginate-Halloysite Nanotube Beads. *Chem. Engineer. J.* **2012**, *187*, 210-216.

[37] Luo, Z. Q.; Song, H. Z.; Feng, X. R.; Run, M. T.; Cui, H. H.; Wu, L. C.; Gao, J. G.; Wang, Z. G. Liquid Crystalline Phase Behavior and Sol–Gel Transition in Aqueous Halloysite Nanotube Dispersions. *Langmuir* **2013**, *29*, 12358–12366.

[38] Feitosa, E.; Brazolin, M. R. S.; Naal, R. M. Z. G.; Lama, M. P. F. M. D.; Lopes, J. R.; Loh, W.; Vasilescu, M. Structural Organization of Cetyltrimethylammonium Sulfate in Aqueous Solution: The Effect of Na_2SO_4. *J. Colloid Interface Sci.* **2006**, *299*, 883–889.

[39] Frank, F. On the Theory of Liquid Crystals. *Discuss. Faraday Soc.* **1958**, *25*, 19-28.

[40] Zhang, S.; Terentjev, E.; Donald, A. Optical Microscopy Study for Director Patterns around Disclinations in Side-Chain Liquid Crystalline Polymer Films. *J. Phys. Chem. B* **2005**, 109, 13195-13199

[41] Mashkour, M.; Kimura, T.; Kimura, F.; Mashkour, M.; Tajvidi, M. Tunable Self-Assembly of Cellulose Nanowhiskers and Polyvinyl Alcohol Chains Induced by Surface Tension Torque. *Biomacromolecules* **2014**, *15*, 60−65.

[42] Onsager, L. The Effects of Shape on the Interaction of Colloidal Particles. *Ann. N.Y. Acad. Sci.* **1949**, *51*, 627-659.

[43] Zhang, S. J.; Kinloch, I. A.; Windle, A. H. Mesogenicity Drives Fractionation in Lyotropic Aqueous Suspensions of Multiwall Carbon Nanotubes. *Nano Lett.* **2006**, *6*, 568-572.

[44] Fustin, C. A.; Glasser, G.; Spiess, H. W.; Jonas, U. Parameters influencing the templated growth of colloidal crystals on chemically patterned surfaces. *Langmuir* **2004**, *20*, 9114-9123.

ACCEPTED MANUSCRIPT

[45] Ahmed, W.; Glass, C.; Kooij, E.; van Ruitenbeek, J. Tuning the Oriented Deposition of Gold Nanorods on Patterned Substrates. *Nanotechnology* **2014**, *25*, 035301.

ACCEPTED MANUSCRIPT

Graphical abstract

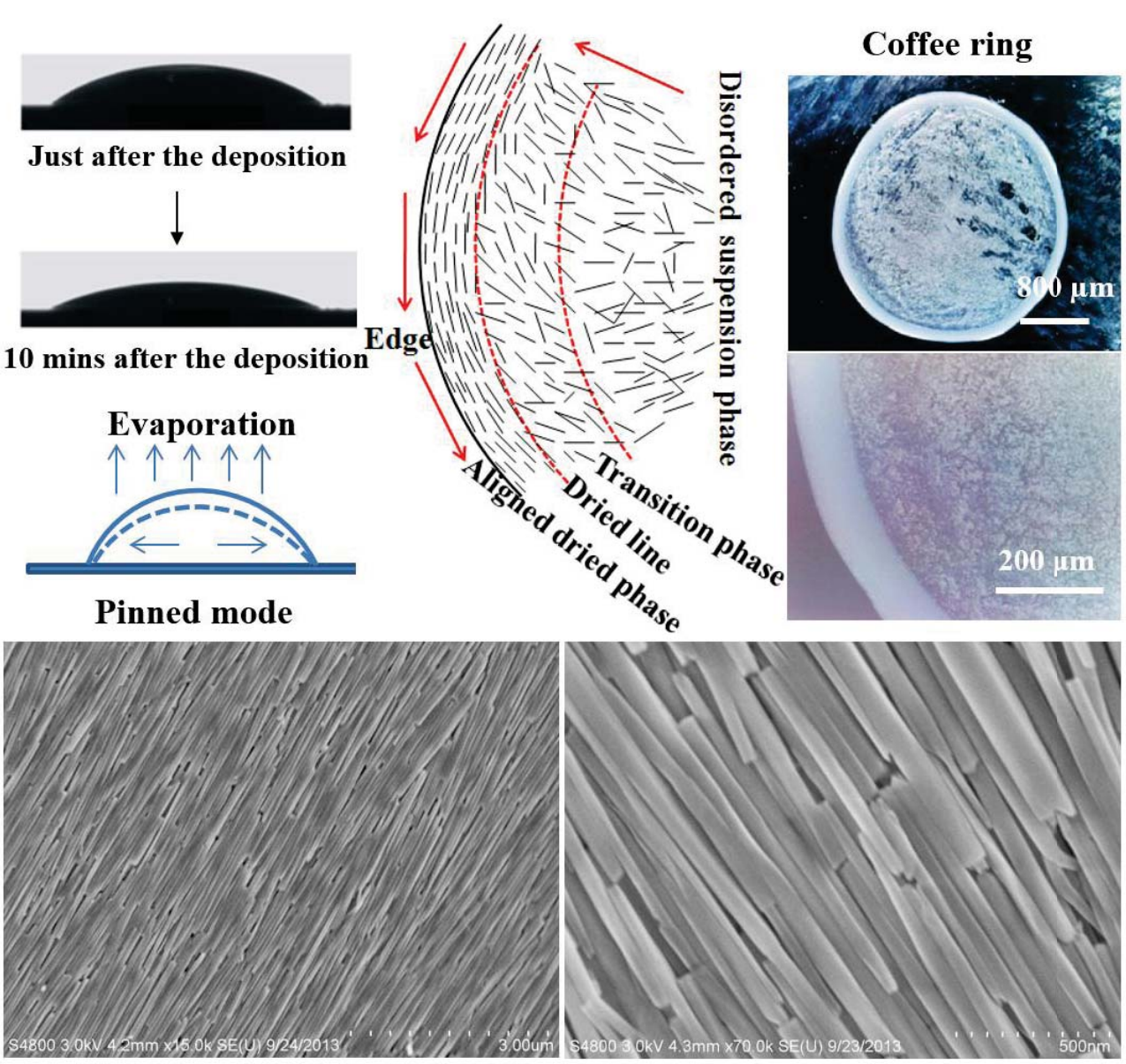

ACCEPTED MANUSCRIPT

Highlights

- Droplet of dispersed charged clay evaporates with tubes oriented in meniscus.
- Liquid crystalline phase aligns tubes at the edge with concentration increase.
- Concentration, pH, length and tube charge were optimized with Onsager's theory.

ACCEPTED MANUSCRIPT